J Mater Sci (2022) 57:553–562

Energy materials

Tunable magnetocaloric effect in amorphous Gd-Fe-Co-Al-Si alloys

Natalia Lindner[1], Zbigniew Śniadecki[2,*], Mieszko Kołodziej[2], Jean-Marc Grenèche[3], Jozef Marcin[4], Ivan Škorvánek[4], and Bogdan Idzikowski[2]

[1] Faculty of Physics, Adam Mickiewicz University, Uniwersytetu Poznańskiego 2, 61-614 Poznań, Poland
[2] Institute of Molecular Physics, Polish Academy of Sciences, M. Smoluchowskiego 17, 60-179 Poznań, Poland
[3] Institut des Molécules et Matériaux du Mans, UMR CNRS 6283, IMMM, Le Mans Université, 72085 Le Mans, France
[4] Institute of Experimental Physics, Slovak Academy of Sciences, Watsonova 47, 040 01 Košice, Slovakia

Received: 29 June 2021
Accepted: 11 October 2021
Published online: 3 January 2022

ABSTRACT

A magnetocaloric effect with wide tunability was observed in melt-spun amorphous $Gd_{65}Fe_{15-x}Co_{5+x}Al_{10}Si_5$ (x = 0, 5, 10) alloys of different Fe/Co ratios. Their magnetic properties were compared with those of the previously investigated parent alloy $Gd_{65}Fe_{10}Co_{10}Al_{15}$. The glassy structure of the melt-spun samples was confirmed by X-ray diffraction (XRD) and ^{57}Fe Mössbauer spectrometry. Their Curie temperatures (T_C) were between 155 and 195 K and increased significantly with decreasing Co content. The highest value of the magnetic entropy change $\Delta S_M = -6.8$ J/kg K was obtained for $Gd_{65}Fe_5Co_{15}Al_{10}Si_5$, when the magnetic field was increased from 0 to 5 T. Refrigerant capacity (RC) takes values close to 700 J/kg for the whole series of the alloys. The occurrence of the second-order phase transition and the conformity of the magnetic behavior with the mean field model were concluded on the basis of the analysis of the universal curves and the values of the exponent n ($\Delta S_M \propto H^n$).

Handling Editor: P. Nash.

Address correspondence to E-mail: sniadecki@ifmpan.poznan.pl

https://doi.org/10.1007/s10853-021-06611-9

GRAPHICAL ABSTRACT

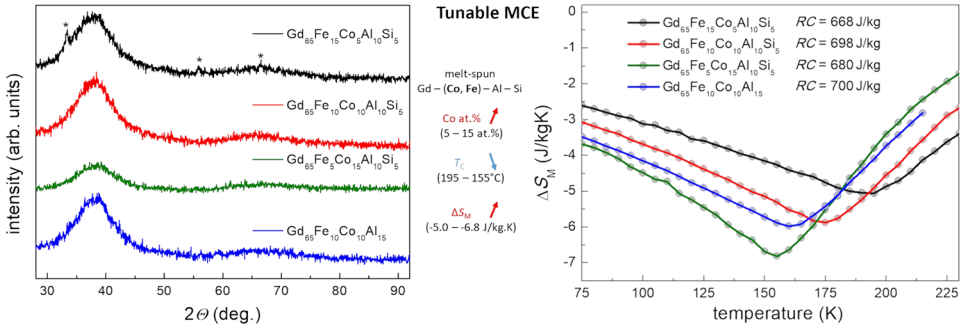

Introduction

The magnetocaloric effect (MCE), discovered in 1881 by Warburg [1], results in temperature changes in a magnetic material subjected to an external magnetic field. Interest in magnetic refrigeration, alternative to the commonly applied refrigeration techniques, has increased since the discovery of the giant magnetocaloric effect (GMCE) in 1997 in the compound $Gd_5Si_2Ge_2$ [2]. This physical phenomenon has been widely studied mainly in intermetallic compounds and in many classes of materials with different chemical compositions. However, current research driven by a strong demand for magnetic cooling as an environmentally friendly and efficient technology, focuses on systems such as amorphous and nanostructured bulk materials, as well as thin films, multilayers, and quantum dots. The solutions based on these systems are also realizations of the idea of energy harvesting associated with the search for new methods for efficient energy production and cooling or heating processes. There has been great interest in new high performance magnetocaloric materials characterized by high magnetic entropy (ΔS_M) and adiabatic temperature changes (ΔT_{ad}).

Pure gadolinium is a typical example of MCE material, mainly due to its Curie temperature of 293 K, which is close to room temperature, and its rather high magnetocaloric performance. Nowadays, it remains the material of choice for studying the efficiency of semi-commercial magnetic refrigerators [3, 4]. Materials undergoing magnetostructural transition [5] and other crystalline materials [6, 7] have recently been extensively studied and are still of high importance. On the other hand, rare earth-based oxides have become an important new area of exploration in the search for new magnetocaloric materials [8, 9]. Recently, vitreous materials [10–13] have also emerged as attractive research objects due to a combination of excellent soft magnetic properties, corrosion resistance, nearly zero magnetic hysteresis losses and their considerable ability to tune Curie temperatures [14–16]. Since the Curie temperature can be generally specified as a midpoint of the useful temperature range for magnetocaloric applications of materials undergoing a second-order magnetic transition, the tunability is defined as the magnitude of changes in the critical temperature with changing composition. Moreover, most amorphous systems exhibit a second-order magnetic phase transition with a significant broadening of the peak in the temperature dependence of magnetic entropy changes [17], due to the presence of chemical and topological disorder. The refrigerant capacity (RC) is calculated from the width and height of the $\Delta S_M(T)$ peak. In general, the RC is directly proportional to the amount of energy, which can be acquired from the magnetocaloric material and is one of the key parameters determining its applications. It is maximized by increasing the value of the full width at half maximum of the magnetic entropy changes (δ_{fwhm}) and the value of the magnetic entropy changes at the transition temperature (ΔS_M^{pk}). Usually, the RC of soft

magnetic amorphous materials is much higher than that of their crystalline counterparts. Although, the values of ΔS_M^{pk} for amorphous materials are lower than those of crystalline systems [2, 14, 18], a higher RC and excellent mechanical properties still make them attractive candidates for further studies as candidates for magnetic refrigeration systems. The magnetic and magnetocaloric properties of a large number of amorphous Gd-based alloys, such as $Gd_{65-x}RE_xFe_{20}Al_{15}$ (x = 0–20, RE = Tb, Dy, Ho, Er) [19], $Gd_{65}Mn_{35-x}Ge_x$ (x = 0, 5, 10) [20], $Gd_{60}X_{30}In_{10}$ (X = Mn, Co, Ni, Cu) [16], $Gd_{55}Co_{20}Al_{24.5}Si_{0.5}$ [12] and $Gd_{55}Fe_xAl_{45-x}$ (x = 15–35) [21], have already been studied.

The aim of our study was to combine the well-known advantages of Gd-based magnetocaloric systems with those of disordered structures in the amorphous alloys of $Gd_{65}Fe_{15-x}Co_{5+x}Al_{10}Si_5$ (x = 0, 5, 10) and compare their pure magnetic and magnetocaloric properties with those of $Gd_{65}Fe_{10}Co_{10}Al_{15}$ parent alloy, previously described in [22]. Si was substituted with the aim of improving the glass forming ability of Gd-Fe-Co-Al alloys. Particular attention is given to the analysis of the critical behavior and to the master curve calculations [23].

Experimental details

The Gd-Co-Fe-(Al, Si) pre-alloys were synthesized by arc-melting in Ar atmosphere from high purity (3 N or more) elements. The ingots were repeatedly melted to ensure their homogeneity. The ribbons were prepared by the melt-spinning technique under Ar atmosphere at a wheel surface velocity of 42 m/s. The structural properties were analyzed by X-ray diffraction (XRD) using a TUR M-62 with HZG 4 goniometer in Bragg–Brentano geometry (Co K_α radiation). The thermal behavior of the alloys was studied by differential scanning calorimetry (DSC) using a Netzsch DSC 404 apparatus at the heating rate q equal to 20 K/min in the temperature range from 50 to 600 °C. Magnetic field dependencies of magnetization were measured with a Physical Property Measurement System (PPMS) using the vibrating sample magnetometer option (VSM). The $M(H)$ dependences were used to calculate the magnetic entropy changes ΔS_M (using Maxwell relation) and in further analysis (*e.g.*, master curves). The RC values were determined from the $-\Delta S_M(T,H)$ dependences [24]. The hyperfine structures at ^{57}Fe sites were investigated by the ^{57}Fe transmission Mössbauer spectrometry to obtain information on the local ^{57}Fe environment at the atomic scale. The spectra were obtained at 300 K using an electromagnetic transducer with a triangular velocity form and a ^{57}Co/Rh γ-ray source. The samples were in the form of a thin powder containing about 5 mg Fe/cm^2 obtained from ribbons after crushing them by hand to reduce texture and internal stress effects. The hyperfine structure was modeled by means of the least-square fitting procedure involving quadrupolar doublets composed of Lorentzian lines using 'MOSFIT' program developed at Université du Maine.

Results and discussion

The X-ray diffraction patterns (Fig. 1) are typical of amorphous systems for all the alloys investigated in the as-quenched state, except for $Gd_{65}Fe_{15}Co_5Al_{10}Si_5$, whose diffractogram showed small reflections marked by stars from an unidentified phase (most probably Gd-rich [25]).

The differential scanning calorimetry curves measured in isochronal mode at a heating rate equal to 20 K/min are shown in Fig. 2. There are two distinct exothermic events above 300 °C for each sample, but other additional shallow and wide peaks are also visible. In general, the Si-containing samples are

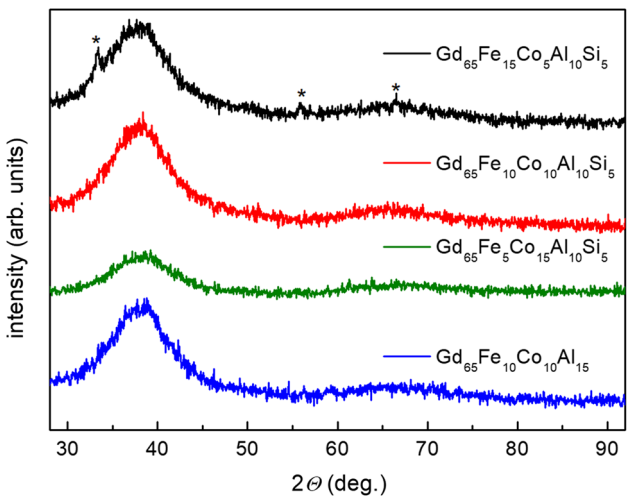

Figure 1 X-ray diffraction (XRD) patterns for as-quenched $Gd_{65}Fe_{15-x}Co_{5+x}Al_{10}Si_5$ (x = 0, 5, 10) and $Gd_{65}Fe_{10}Co_{10}Al_{15}$ alloys.

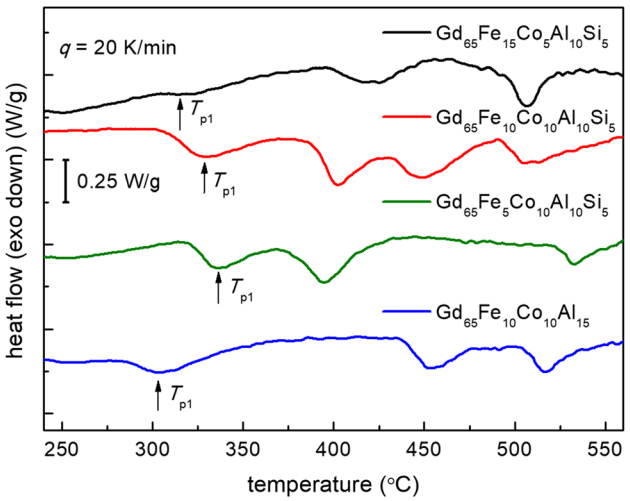

Figure 2 Differential scanning calorimetry (DSC) curves for $Gd_{65}Fe_{15-x}Co_{5+x}Al_{10}Si_5$ (x = 0, 5, 10) and $Gd_{65}Fe_{10}Co_{10}Al_{15}$ alloys measured at the heating rate of q = 20 K/min.

more structurally stable than the parent alloy $Gd_{65}Fe_{10}Co_{10}Al_{15}$ (the first exothermic events are marked by arrows in Fig. 2) and crystallize in a more complex way. The enthalpies of the distinct peaks range from 1 to about 6 J/g. A more detailed analysis of the crystallization processes as well as the study of crystallization products is out of the scope of the present paper. It should simply be noted that $Gd_{65}Fe_{10}Co_{10}Al_{15}$ exhibits the lowest thermal stability (taking into account transition temperatures) from among the studied samples, while for the Si-containing samples the substitution of Fe for Co increases the crystallization temperature (T_{p1}) even more significantly. The low thermal stability of $Gd_{65}Fe_{15}Co_5Al_{10}Si_5$ alloy may be also related to pre-existing nanocrystallites, which may act as crystallization facilitators [26].

The ^{57}Fe Mössbauer spectra recorded at 300 K are shown in Fig. 3. It should be emphasized that the absorption area is quite small (note the relative transmission scale) due to a low content of Fe and a high content of Gd (heavy element and therefore γ-photon absorbing atom). Therefore, the spectrum of $Gd_{65}Fe_5Co_{15}Al_{10}Si_5$ (the lowest Fe content) is not shown here. The quadrupolar hyperfine structures result from line broadening, while their asymmetry depends on the chemical composition. The shape of the experimental lines can be successfully fitted by considering (i) a finite number of quadrupolar components describing independently the quadrupolar splitting and isomer shift, or (ii) a continuous distribution of quadrupolar

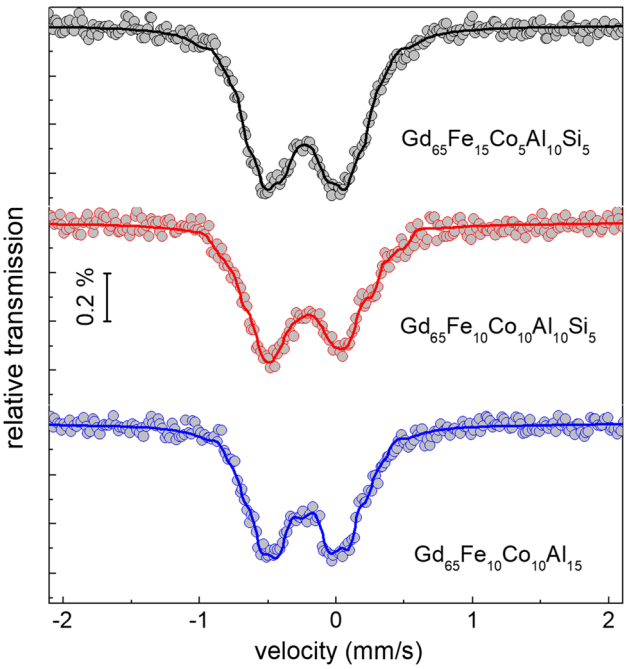

Figure 3 The ^{57}Fe Mössbauer spectra of $Gd_{65}Fe_{15-x}Co_{5+x}Al_{10}Si_5$ (x = 0, 5) and $Gd_{65}Fe_{10}Co_{10}Al_{15}$ amorphous alloys measured at 300 K.

splitting linearly correlated with the isomer shift to reproduce the asymmetry. The parameters obtained from the fit are the mean values of isomer shift and quadrupolar splitting that are independent of the model assumed (see Table 1). The second model is more often applied for the interpretation of the quadrupolar and/or magnetic (Zeeman splitting) ^{57}Fe Mössbauer spectra recorded for the amorphous Fe-containing alloys. The values of $q = (< QS^2 > / < QS >^2)$ which lie in the range 1.22–1.27 (see Table 1) are consistent with the results for an amorphous structure [27]. However, the quadrupolar splitting distributions show two peaks, suggesting that there are two main types of local Fe environments. Indeed, the dominant Gd content relative to the Fe and other atomic species contents suggests that Fe is preferentially surrounded by Gd atoms, but the presence of Co, Al and Si modifies the first coordination shell.

The isothermal magnetization curves of the alloys $Gd_{65}Fe_{15-x}Co_{5+x}Al_{10}Si_5$ (x = 0, 5, 10) and also $Gd_{65}Fe_{10}Co_{10}Al_{15}$ were measured for the magnetic field increase from 0 to 5 T over a wide temperature range. The first quadrants of these hysteresis loops were taken into account to calculate the changes in magnetic entropy, as a function of temperature and magnetic field, using Maxwell's relation [28]:

Table 1 Refined values of hyperfine parameters for amorphous $Gd_{65}Fe_{15-x}Co_{5+x}Al_{10}Si_5$ (x = 0, 5) and $Gd_{65}Fe_{10}Co_{10}Al_{15}$ alloys

Composition	< IS > mm/s ± 0.01	< QS > mm/s ± 0.01	q = $< QS^2 > / < QS >^2$ ± 0.02
$Gd_{65}Fe_{15}Co_5Al_{10}Si_5$	− 0.11	0.54	1.27
$Gd_{65}Fe_{10}Co_{10}Al_{15}$	− 0.11	0.51	1.24
$Gd_{65}Fe_{10}Co_{10}Al_{10}Si_5$	− 0.11	0.53	1.22

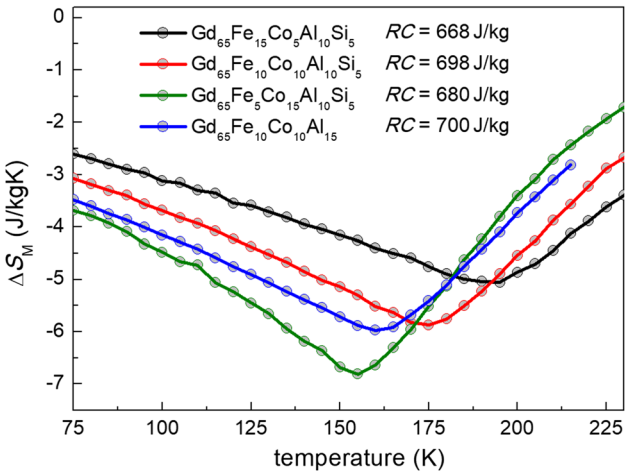

Figure 4 Temperature dependences of magnetic entropy change ΔS_M calculated for melt-spun $Gd_{65}Fe_{15-x}Co_{5+x}Al_{10}Si_5$ (x = 0, 5, 10) and $Gd_{65}Fe_{10}Co_{10}Al_{15}$ alloys from the magnetization isotherms measured up to 5 T.

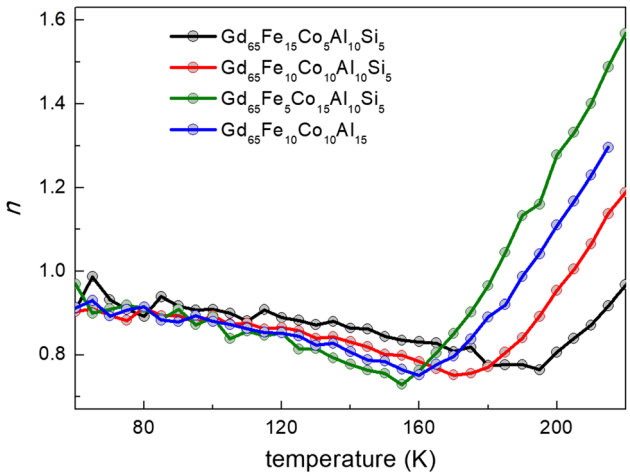

Figure 5 Temperature dependences of exponent n for amorphous $Gd_{65}Fe_{15-x}Co_{5+x}Al_{10}Si_5$ (x = 0, 5, 10) and $Gd_{65}Fe_{10}Co_{10}Al_{15}$ alloys.

$$\Delta S_M = \mu_0 \int_0^{H_{\max}} \left(\frac{dM}{dT}\right)_H dH,$$

where ΔS_M, μ_0, H, T and M represent the change in magnetic entropy, magnetic permeability of vacuum, magnetic field strength, temperature and magnetization, respectively. The curves of $\Delta S_M(T)$ are depicted in Fig. 4 with the calculated RC values. The temperature shift of the magnetic entropy peak ΔS_M^{pk} with stoichiometry is rather significant and naturally associated with changes in T_C. The maximum peaks of the magnetic entropy curves (ΔS_M^{pk}) of the samples studied appear in the range 150–200 K and are correlated with the changes in their T_C temperatures, which depend on the samples stoichiometry. T_C values for $Gd_{65}Fe_5Co_{15}Al_{10}Si_5$, $Gd_{65}Fe_{10}Co_{10}Al_{15}$, $Gd_{65}Fe_{10}Co_{10}Al_{10}Si_5$ and $Gd_{65}Fe_{15}Co_5Al_{10}Si_5$ determined on the basis of $M(T)$ curves measured in $\mu_0 H$ = 0.05 T are equal to 154, 160, 175 and 191 K, while those roughly determined on the basis of $\Delta S_M(T)$ curves are equal to 155, 160, 175 and 195 K, respectively. The maximum values of magnetic entropy changes ($\Delta\mu_0 H$ = 5 T) are varying from -6.8 to -5.0 J/kg K. Such a distinct change in Curie temperature values has been observed for example in $Gd_{60}M_{30}In_{10}$ (M = Mn, Fe, Co, Ni, Cu) [16] and $Fe_{80-x}B_{12}Cr_8Gd_x$ (x = 1, 2, 3, 5, 8, 10, 11) [29], and called the tunable MCE. The refrigerant capacity is calculated as the integral of magnetic entropy changes and is given by the formula [2, 28]:

$$RC = \int_{T_1}^{T_2} |-\Delta S_M(T)| dT,$$

where T_1 and T_2 are the temperatures at half maximum of the ascending and descending parts of the ΔS_M peak, respectively. So, the changes in ΔS_M^{pk} and the shape of $\Delta S_M(H,T)$ are of the highest importance when analyzing the refrigerant capacity. The changes in the shape of the magnetic entropy peaks for the melt-spun ribbons studied are typical of glassy systems, i.e., the peaks broaden, which directly affects the RC values. The refrigerant capacity values of

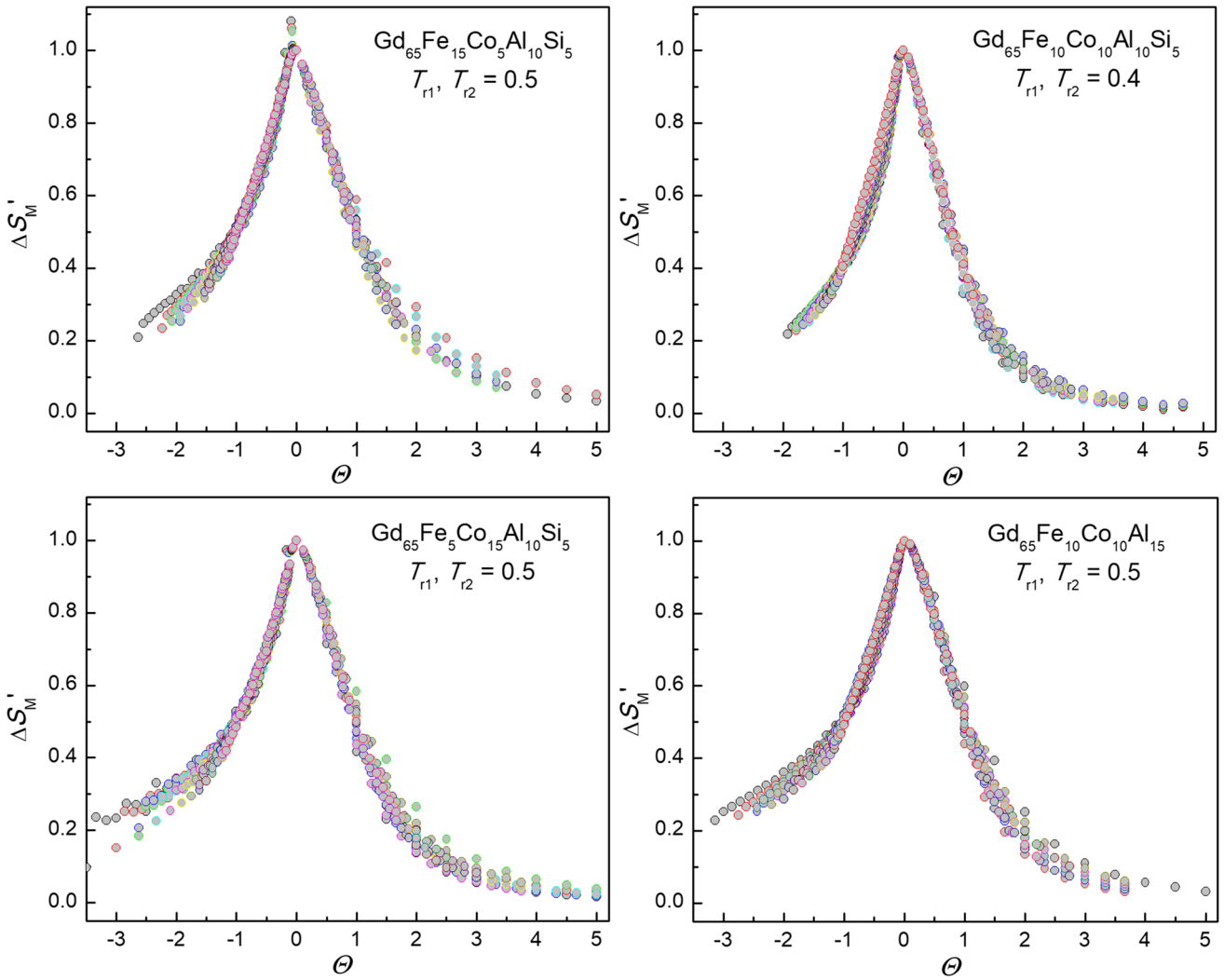

Figure 6 Master curves for the applied magnetic field ranging from 0.2 to 5.0 T determined with temperature step ΔT = 5 K for amorphous $Gd_{65}Fe_{15-x}Co_{5+x}Al_{10}Si_5$ (x = 0, 5, 10) and $Gd_{65}Fe_{10}Co_{10}Al_{15}$ samples.

$Gd_{65}Fe_{15}Co_5Al_{10}Si_5$, $Gd_{65}Fe_5Co_{15}Al_{10}Si_5$ and $Gd_{65}Fe_{10}Co_{10}Al_{10}Si_5$ are equal to 668, 680 and 698 J/kg, respectively. The highest RC was found for $Gd_{65}Fe_{10}Co_{10}Al_{15}$ and equals 700 J/kg. The RC values are comparable with those of the other Gd-based systems, *e.g.*, $Gd_{65}Fe_{20}Al_{15}$ [30] with RC = 726 J/kg, and $Gd_{55}Co_{20}Fe_5Al_{18}Si_5$ [26] with RC = 719 J/kg [31]. This confirms that the presence of nonuniformity of magnetic structure (broad distribution of transition temperature) leads to a reduction in the height of $\Delta S_M(T)$ peak but also to its broadening, which allows easy control of refrigerant capacity.

The field dependence of the magnetic entropy changes can be used to determine the magnetic properties of the alloys in more details and can be expressed in the following form:

$$n = \frac{d\ln|\Delta S_M|}{dlnH}.$$

In general, the field dependence of the magnetic entropy follows a power law of the field, $\Delta S_M \propto H^n$ [23]. The values of the exponent n versus temperature are plotted in Fig. 5. According to the value of the exponent n, the above-mentioned dependence can be divided into three field independent ranges, below, above and at the Curie temperature. For all samples studied, the value of the exponent n is close to 2/3 at T_C, which is in excellent agreement with the mean field theory. Therefore, as expected, it tends to reach 1 at low temperatures and 2 well above T_C [32].

V. Franco et al. [23] have proposed a master curve analysis for materials with a second-order phase

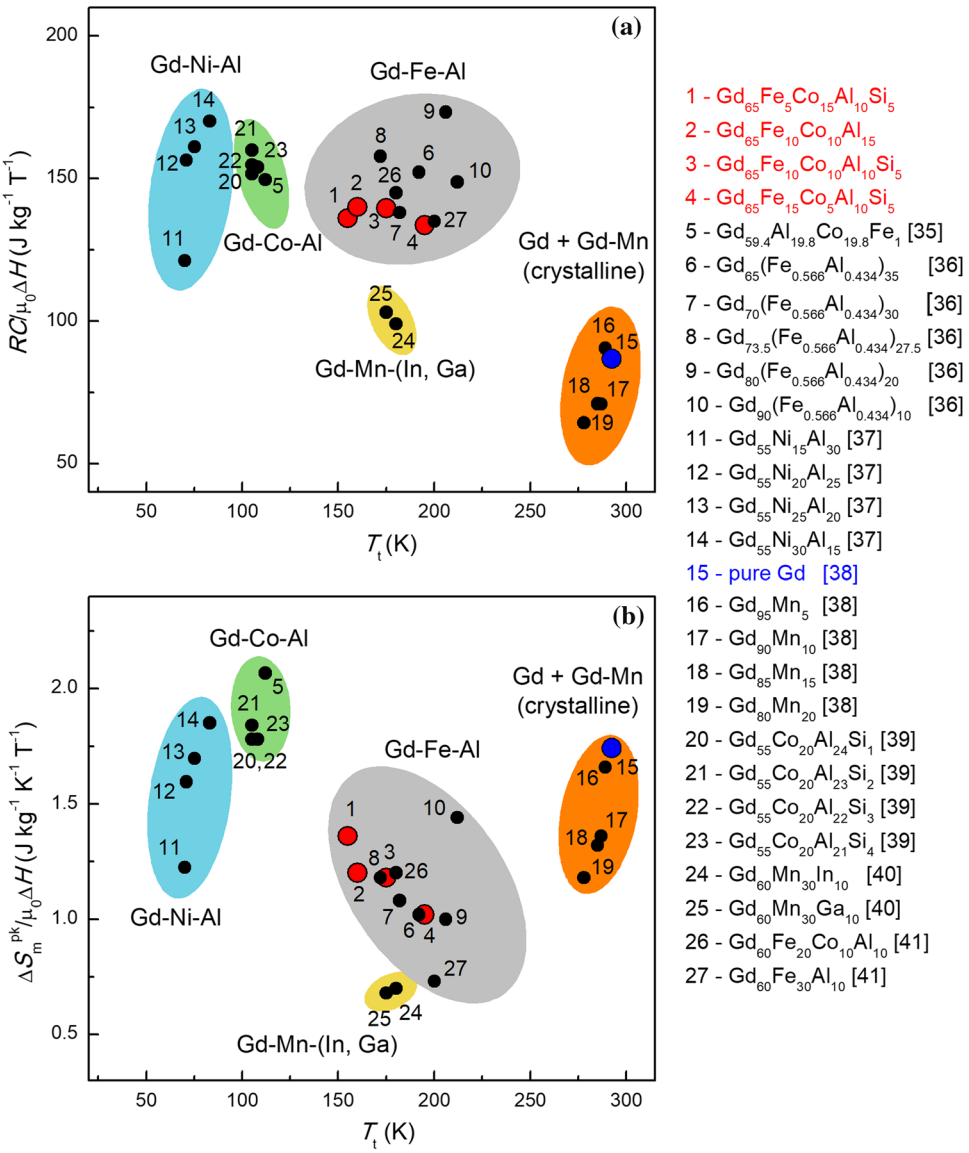

Figure 7 Transition temperature dependences of the refrigerant capacity (**a**) and maximal isothermal magnetic entropy changes (**b**) divided by the magnetic field changes for $Gd_{65}Fe_{15-x}Co_{5+x}Al_{10}Si_5$ (x = 0, 5, 10) and $Gd_{65}Fe_{10}Co_{10}Al_{15}$ alloys (marked by red dots) and various Gd-based amorphous materials from literature (marked by full black dots). The analogous data for the pure Gd and Gd-Mn crystalline alloys are presented for comparison.

transition. C.M. Bonilla et al. [33] have constructed a universal curve for the family of Laves phases and mixed manganites. Furthermore, it has been shown that this approach does not work for the systems with a first-order phase transition. The construction of the phenomenological master curve is based on the normalization of magnetic entropy changes $\Delta S_M'$ in different external magnetic fields into corresponding values of temperature and is given by the formula [23]:

$$\Theta = \begin{cases} -(T - T_C)/(T_{r1} - T_C) T \leq T_C \\ (T - T_C)/(T_{r2} - T_C) T > T_C \end{cases},$$

where T_{r1} and T_{r2} are the reference points for each curve, determined as $0.5\Delta S_M^{pk}$ (except $Gd_{65}Fe_{10}Co_{10}Al_{10}Si_5$, for which better scaling was achieved for $T_{r1} = T_{r2} = 0.4$). The universal curves for Gd-based amorphous alloys are shown in Fig. 6. All master curves collapse for $\Theta > 0$ (in the paramagnetic region) and no deviations were observed. As we have shown [34], deviations at temperatures below the magnetic phase transition may be related, for example, to dynamic magnetic ordering in crystalline compounds. No clear deviations can be observed in Fig. 6, even below $\Theta = 0$, confirming that the phase transition in all analyzed samples is of the second order, as expected for metallic glasses.

To complement the discussion, we present in Fig. 7 a comparison of two characteristic parameters of magnetocaloric materials. The transition temperature

dependences of the refrigerant capacity RC divided by the magnetic field change $\mu_0\Delta H$ (Fig. 7a) and the maximum magnetic entropy changes ΔS_M^{pk} divided by the magnetic field change $\mu_0\Delta H$ (Fig. 7b) are shown for the alloys studied (red dots), for various Gd-based metallic glasses described in the literature, for pure Gd and Gd–Mn crystalline alloys for comparison. The $\mu_0\Delta H$ divisor was applied to remove the magnetic field effect, but it should be kept in mind that the magnetic field dependences of the magnetic entropy changes and the refrigerant capacity are not linear in the whole $\mu_0 H$ range. Nevertheless, such a comparison has revealed some additional information about the possible performance of the examined alloys. The most important conclusion that can be drawn from Fig. 7 is the significant impact of transition metal and simple metal substitutions not only on the values of magnetic entropy changes and refrigerant capacity but also on the values of transition temperatures. It was also confirmed that the small variations in chemical composition can allow the Curie temperature to be tuned over a wide range.

Conclusions

The thermal stability, structural, magnetic and magnetocaloric properties of the melt-spun alloys $Gd_{65}Fe_{15-x}Co_{5+x}Al_{10}Si_5$ (x = 0, 5, 10) were determined and compared to the properties of the parent alloy $Gd_{65}Fe_{10}Co_{10}Al_{15}$ [22]. The samples of the melt-spun alloys unambiguously exhibit amorphous structures as confirmed by X-ray diffraction, except for $Gd_{65}Fe_{15}Co_5Al_{10}Si_5$, in which a small volume fraction of crystalline phase was detected. The Curie temperatures, determined on the basis of temperature dependences of magnetic entropy changes, range from 155 to 195 K for the analyzed samples. The substitution by metalloid atoms can be used to tune the Curie temperature, simultaneously causing insignificant changes in the other magnetic or magnetocaloric properties. On the other hand, changes in the Fe/Co ratio are well established to play an indispensable role in inducing changes in the critical temperature, mainly due to alterations in the exchange integral according to the Bethe-Slater curve [42]. The peaks of the variations of magnetic entropy with temperature are very broad which can be considered as an advantage, as it could allow a wider working temperature range for these magnetocaloric materials. The refrigerant capacities are close to 700 J/kg for all the investigated alloys. Although the maximum value of magnetic entropy changes for amorphous alloys, it is slightly lower than that of crystalline systems: this high RC makes glassy ribbons attractive for further investigation in terms of possible applications, *e.g.*, in magnetic refrigerators. All the analyzed alloys exhibit the second-order phase transitions and magnetic behavior consistent with the mean field model, as confirmed by the universal curves and the n exponent analysis.

Acknowledgements

The group at the Institute of Experimental Physics SAS acknowledges support of the projects VEGA 2/0171/19 and APVV-19-0369.

Data availability

The raw/processed data required to reproduce these findings cannot be shared freely at this time as the data also form part of an ongoing study, but can be shared on request.

Declarations

Conflict of interest The authors declare that they have no known competing financial interests or personal relationships that could have appeared to influence the work reported in this paper.

References

[1] Warburg E (1881) Magnetische Untersuchungen. Ueber einige Wirkungen der Coercitivkraft. Ann Phys (Leipz) 249:141–164

[2] Pecharsky VK, Gschneidner KA Jr (1997) Giant magnetocaloric effect in $Gd_5Si_2Ge_2$. Phys Rev Lett 78:3–6. https://doi.org/10.1103/PhysRevLett.78.4494

[3] Pecharsky VK, Gschneidner KA Jr (2000) Magnetocaloric materials. Ann Rev Mater Sci 30:387–429. https://doi.org/10.1146/annurev.matsci.30.1.387

[4] Ćwik J (2013) Effect of partial Gd substitution on the magnetic and magnetocaloric properties in Dy-Ho-Gd-Co multicomponent compounds. Phys Stat Sol b 250:1926–1931. https://doi.org/10.1002/pssb.201349074

[5] Gamzatov AG, Aliev AM, Batdalov AB, Khizriev SK, Kuzmin DA, Kamantsev AP, Kim DH, Yen NH, Dan NH, Yu SC (2021) Dynamics of the magnetocaloric effect in cyclic magnetic fields in $Ni_{50}Mn_{35}Al_2Sn_{13}$ ribbon sample. J Mater Sci 56:15397–15406. https://doi.org/10.1007/s10853-021-06257-7

[6] Li L, Yan M (2020) Recent progresses in exploring the rare earth based intermetallic compounds for cryogenic magnetic refrigeration. J Alloys Compd 823:153810. https://doi.org/10.1016/j.jallcom.2020.153810

[7] Ma Z, Dong X, Zhang Z, Li L (2021) Achievement of promising cryogenic magnetocaloric performances in $La_{1-x}Pr_xFe_{12}B_6$ compounds. J Mater Sci Technol 92:138–142. https://doi.org/10.1016/j.jmst.2021.02.055

[8] Li L, Xu P, Ye S, Li Y, Liu G, Huo D, Yan M (2020) Magnetic properties and excellent cryogenic magnetocaloric performances in B-site ordered RE_2ZnMnO_6 (RE = Gd, Dy and Ho) perovskites. Acta Mater 194:354–365. https://doi.org/10.1016/j.actamat.2020.05.036

[9] Wu B, Zhang Y, Guo D, Wang J, Ren Z (2020) Structure, magnetic properties and cryogenic magneto-caloric effect (MCE) in RE_2FeAlO_6 (RE = Gd, Dy, Ho) oxides. Ceram Int 47:6290–6297. https://doi.org/10.1016/j.ceramint.2020.10.207

[10] Dey S, Roy RK, Mallick AB, Mitra A, Panda AK (2019) High-temperature magnetocaloric effect in devitrified Fe/Co based glassy monolayer and bilayer ribbons. J Mater Sci 54:11292–11303. https://doi.org/10.1007/s10853-019-03684-5

[11] Wang YM, Guo D, Wu BB, Geng SH, Zhang YK (2020) Magnetocaloric effect and refrigeration performance in $RE_{60}Co_{20}Ni_{20}$ (RE = Ho and Er) amorphous ribbons. J Magn Magn Mater 498:166179. https://doi.org/10.1016/j.jmmm.2019.166179

[12] Xue L, Shao LL, Luo Q, Hu LN, Zhao YB, Yin KB, Zhu MY, Sun LT, Shen BL, Bian XF (2021) Liquid dynamics and glass formation of $Gd_{55}Co_{20}Al_{25}$ metallic glass with minor Si addition. J Mater Sci Technol 77:28–37. https://doi.org/10.1016/j.jmst.2020.11.024

[13] Xue L, Luo Q, Shao LL, Shen BL (2020) Magnetocaloric difference between ribbon and bulk shape of Gd-based metallic glasses. J Magn Magn Mater 497:166015. https://doi.org/10.1016/j.jmmm.2019.166015

[14] Ucar H, Ipus JJ, Franco V, McHenry ME, Laughlin DE (2012) Overview of amorphous and nanocrystalline magnetocaloric materials operating near room temperature. JOM 64:782–788. https://doi.org/10.1007/s11837-012-0349-6

[15] Inoue A, Takeuchi A (2011) Recent development and application products of bulk glassy alloys. Acta Mater 59:2243–2267. https://doi.org/10.1016/j.actamat.2010.11.027

[16] Mayer C, Gorsse S, Ballon G, Caballero-Flores R, Franco V, Chevalier B (2011) Tunable magnetocaloric effect in Gd-based glassy ribbons. J Appl Phys 110:053920. https://doi.org/10.1063/1.3632983

[17] Gębara P, Pawlik P, Škorvánek I, Bednarcik J, Marcin J, Michalik Š, Donges J, Wysłocki JJ, Michalski B (2014) Effect of Al content on the order of phase transition and magnetic entropy change in $LaFe_{11}Co_{0.8}(Si_{1-x}Al_x)_{1.2}$ alloys. J Magn Magn Mater 372:201–207. https://doi.org/10.1016/j.jmmm.2014.07.053

[18] Synoradzki K, Das D, Frąckowiak A, Szymański D, Skokowski P, Kaczorowski D (2019) Study on magnetocaloric and thermoelectric application potential of ferromagnetic compound $CeCrGe_3$. J Appl Phys 126:075114. https://doi.org/10.1063/1.5107450

[19] Fang YK, Chen HC, Hsieh CC, Chang HW, Zhao XG, Chang WC, Li W (2011) Structures and magnetocaloric effects of $Gd_{65-x}RE_xFe_{20}Al_{15}$ (x = 0–20; RE = Tb, Dy, Ho, and Er) ribbons. J Appl Phys 109:15–18. https://doi.org/10.1063/1.3561447

[20] Zhong XC, Min JX, Zheng ZG, Liu ZW, Zeng DC (2012) Critical behavior and magnetocaloric effect of $Gd_{65}Mn_{35-x}Ge_x$ (x = 0, 5, and 10) melt-spun ribbons. J Appl Phys 112:1–6. https://doi.org/10.1063/1.4740062

[21] Yuan F, Li Q, Shen B (2012) The effect of Fe/Al ratio on the thermal stability and magnetocaloric effect of $Gd_{55}Fe_xAl_{45-x}$ (x = 15–35) glassy ribbons. J Appl Phys 111:1–4. https://doi.org/10.1063/1.3677780

[22] Pierunek N, Śniadecki Z, Marcin J, Škorvánek I, Idzikowski B (2014) Magnetocaloric Effect of Amorphous

$Gd_{65}Fe_{10}Co_{10}Al_{10}X_5$ (X = Al, Si, B) Alloys, IEEE Trans. Magn 50:11–14. https://doi.org/10.1109/TMAG.2014.2318595

[23] Franco V, Blázquez JS, Conde A (2006) Field dependence of the magnetocaloric effect in materials with a second order phase transition: a master curve for the magnetic entropy change. Appl Phys Lett 89:10–13. https://doi.org/10.1063/1.2399361

[24] Pecharsky VK, Gschneidner KA (1999) Magnetocaloric effect from indirect measurements: magnetization and heat capacity. J Appl Phys 86:565–575. https://doi.org/10.1063/1.370767

[25] Gorsse S, Chevalier B, Orveillon G (2008) Magnetocaloric effect and refrigeration capacity in $Gd_{60}Al_{10}Mn_{30}$ nanocomposite. Appl Phys Lett 92:122501. https://doi.org/10.1063/1.2884326

[26] Atalay S, Gencer H, Kaya AO, Kolat VS, Izgi T (2013) Influence of Si substitution on the structural, magnetic and magnetocaloric properties of $Gd_{55}Co_{20}Fe_5Al_{20-x}Si_x$ alloys. J Non Cryst Solids 365:99–104. https://doi.org/10.1016/j.jnoncrysol.2013.01.042

[27] Lopez-Herrera ME, Greneche JM, Varret F (1983) Analysis of the Mössbauer quadrupole spectra of some amorphous fluorides Phys. Rev B 28:4944–4948. https://doi.org/10.1103/PhysRevB.28.4944

[28] Franco V, Blazquez JS, Millan M, Borrego JM, Conde CF, Conde A (2007) The magnetocaloric effect in soft magnetic amorphous alloys. J Appl Phys 101:09C503. https://doi.org/10.1063/1.2709409

[29] Law JY, Ramanujan RV, Franco V (2010) Tunable Curie temperatures in Gd alloyed Fe-B-Cr magnetocaloric materials. J Alloys Compd 508:14–19. https://doi.org/10.1016/j.jallcom.2010.08.049

[30] Dong QY, Shen BG, Chen J, Shen J, Wang F, Zhang HW, Sun JR (2009) Large magnetic refrigerant capacity in $Gd_{71}Fe_3Al_{26}$ and $Gd_{65}Fe_{20}Al_{15}$ amorphous alloys. J Appl Phys 105:053908. https://doi.org/10.1063/1.3072631

[31] Bebenin NG, Zainullina RI, Ustinov VV, Mukovskii YM (2012) Effect of inhomogeneity on magnetic, magnetocaloric, and magnetotransport properties of $La_{0.6}Pr_{0.1}Ca_{0.3}MnO_3$ single crystal. J Magn Magn Mater 324:1112–1116. https://doi.org/10.1016/j.jmmm.2011.10.043

[32] Franco V, Conde A (2010) Scaling laws for the magnetocaloric effect in second order phase transitions: from physics to applications for the characterization of materials. Int J Refrig 33:465–473. https://doi.org/10.1016/j.ijrefrig.2009.12.019

[33] Bonilla CM, Herrero-Albillos J, Bartolomé F, García LM, Parra-Borderías M, Franco V (2010) Universal behavior for magnetic entropy change in magnetocaloric materials: an analysis on the nature of phase transitions. Phys Rev B 81:224424. https://doi.org/10.1103/PhysRevB.81.224424

[34] Pierunek N, Śniadecki Z, Werwiński M, Wasilewski B, Franco V, Idzikowski B (2017) Normal and inverse magnetocaloric effects in structurally disordered Laves phase $Y_{1-x}Gd_xCo_2$ ($0 \leq x \leq 1$) compounds. J Alloys Compd 702:258–265. https://doi.org/10.1016/j.jallcom.2017.01.181

[35] Liu J, Wang Q, Wu M, Zhang Y, Shen H, Ma W (2017) Improving the refrigeration capacity of Gd-rich wires through Fe-doping. J Alloys Compd 711:71–76. https://doi.org/10.1016/j.jallcom.2017.03.363

[36] Zhang L, Bao M, Zheng Q, Tian L, Du J (2016) Magnetocaloric effect in high Gd content Gd-Fe-Al based amorphous/nanocrystalline systems with enhanced Curie temperature and refrigeration capacity. AIP Adv 6:035220. https://doi.org/10.1063/1.4945407

[37] Yuan F, Du J, Shen B (2012) Controllable spin-glass behavior and large magnetocaloric effect in Gd-Ni-Al bulk metallic glasses. Appl Phys Lett 101:032405. https://doi.org/10.1063/1.4738778

[38] Jayaraman TV, Boone L, Shield JE (2013) Magnetocaloric effect and refrigerant capacity in melt-spun Gd–Mn alloys. J Magn Magn Mater 345:153–158. https://doi.org/10.1016/j.jmmm.2013.06.016

[39] Li Q, Shen B (2011) Glass-forming ability and magnetocaloric effect in $Gd_{55}Co_{20}Al_{25-x}Si_x$ bulk metallic glass. IEEE Trans Magn 47:2490–2493. https://doi.org/10.1109/TMAG.2011.2160332

[40] Mayer C, Chevalier B, Gorsse S (2010) Magnetic and magnetocaloric properties of the ternary Gd-based metallic glasses $Gd_{60}Mn_{30}X_{10}$, with X = Al, Ga, In. J Alloys Compd 507:370–375. https://doi.org/10.1016/j.jallcom.2010.07.210

[41] Schwarz B, Podmilsak B, Mattern N, Eckert J (2010) Magnetocaloric effect in Gd-based $Gd_{60}Fe_xCo_{30}$-xAl_{10} metallic glasses. J Magn Magn Mater 322:2298–2303. https://doi.org/10.1016/j.jmmm.2010.02.029

[42] Fang YN, Hahn H, Kobe S, Witte R, Singh SP, Feng T, Ghafari M (2019) Modifying the transition temperature, 120 K $\leq$ Tc $\leq$ 1150 K, of amorphous $Fe_{90-x}Co_xSc_{10}$ with simultaneous alteration of fluctuation of exchange integral up to zero. Sci Rep 9:412. https://doi.org/10.1038/s41598-018-36891-2